

# TEM study of Mg-Zn precipitates in Mg-Zn-Y alloys

J. C. RAO\*, M. SONG, K. FURUYA

High Voltage Electron Microscopy Station, National Institute for Materials Science, 3-13 Sakura, Tsukuba, Ibaraki 305-0003, Japan  
E-mail: jcr Rao@hit.edu.cn

S. YOSHIMOTO, M. YAMASAKI, Y. KAWAMURA

21st Century COE Program, Graduate School of Science and Technology, Kumamoto University, 2-39-1 Kurokami, Kumamoto 860-8555, Japan

Published online: 17 April 2006

The precipitates in Mg-Zn-Y alloys in the as-cast state with nominal atomic composition of  $Mg_{96}Zn_1Y_3$ ,  $Mg_{96}Zn_2Y_2$  and  $Mg_{97}Zn_1Y_2$  were studied by means of TEM as well as XRD techniques. The results show that there is a phase separation of Zn on the nanometer scale in these alloys. Two kinds of nano-sized precipitates were found, namely MgZn and  $MgZn_2$ . TEM observation shows that MgZn precipitates are distributed in both the Mg matrix and in  $Mg_{24}Y_5$  grains, which is the typical precipitate in Mg-Zn-Y alloys. There is an inherent crystallographic relationship between MgZn and  $Mg_{24}Y_5$  precipitates:  $[1\bar{1}0]_{MgZn} // [1\bar{1}2]_{Mg_{24}Y_5}$ ,  $(11\bar{3})_{MgZn} // (330)_{Mg_{24}Y_5}$ . The size of  $MgZn_2$  precipitates is much smaller than that of MgZn precipitates. They are distributed only in  $Mg_{24}Y_5$  grains, not in the Mg matrix. It is suggested that the nano-sized precipitates, MgZn and  $MgZn_2$ , can improve the mechanical properties of the Mg-Zn-Y alloys studied. © 2006 Springer Science + Business Media, Inc.

## 1. Introduction

The application of cast magnesium components in vehicles, communication equipment and hand tools has been increasing over recent decades and will continue to increase in the future [1–4]. A number of commercial magnesium casting alloys are based on the Mg-Zn binary alloy system with minor additions of rare earth (RE) elements. The rare earth additions are known to improve the casting characteristics and elevated temperature strength [5–7]. High-performance rapidly solidified powder metallurgy (RS P/M) Mg-Zn-Y alloys have been developed by Kawamura *et al.* [8]. The nanocrystalline Mg-Zn-Y alloy, prepared by warm extrusion of rapidly solidified powders at 573 K, has excellent mechanical properties including a maximum tensile yield strength of about 600 MPa and elongation of about 5% at room temperature [8, 9]. There are some reports of a kind of long periodic stacking (LPS) phase, for example, 6H-type LPS phase [8–12], together with hexagonal close-packed (*hcp*) 2H-Mg fine grain substrate. Several kinds of precipitates were initiated from a supersaturated solid solution of Zr and Y in 2H-Mg by segregation of Zn and/or Y atoms. [1, 13]. It is well estab-

lished that Al-Mg alloys achieve a combination of good mechanical properties and formability through solid solution strengthening [14] and that trace additions of Ag ( $\sim 0.4$  mass%) stimulate precipitation behavior in all Al alloys containing Mg, with an acceleration in the kinetics of the age-hardening response and an increase in the maximum hardness achievable [15]. To investigate the effect of precipitates on the mechanical properties in pseudo ternary Mg-Zn-Y alloys, in the present work, the evolution of precipitates in the ingots of these alloys has been studied by transmission electron microscopy (TEM) and X-ray diffraction (XRD) analysis.

## 2. Experimental

The Mg-Zn-Y pseudo ternary alloy ingots, with nominal atomic composition of  $Mg_{96}Zn_1Y_3$ ,  $Mg_{96}Zn_2Y_2$  and  $Mg_{97}Zn_1Y_2$  (at.%), were prepared by induction melting of the mixture of pure metals in an argon atmosphere. Rapidly Solidified (RS) powders were produced by He-gas atomization at a dynamic gas pressure of 0.98 MPa, and at a molten-alloy temperature of 1048 K. Sieved

\*Author to whom all correspondence should be addressed.

## CHARACTERIZATION OF REAL MATERIALS

powders with diameters less than  $32\ \mu\text{m}$  were first cold pressed into a copper can and then degassed for 900 s at room temperature. The TEM samples were sectioned both longitudinally and transversely relative to the process direction. They were then prepared by conventional mechanical grinding, followed by ion thinning using a JIT-100 Ion Beam Thinner at 4 kV. The TEM observations were carried out in a JEM 2000FX operating at 200 kV and a JEM 4000EX at 400 kV.

### 3. Results and discussion

The evolution of microstructure in Mg-Zn-Y alloy ingots has been studied in detail with TEM as well as XRD techniques. Two new phases, MgZn and MgZn<sub>2</sub>, were identified by XRD analysis in the studied alloys as well as the typical Mg<sub>24</sub>Y<sub>5</sub> and LPS phase (for example, Mg<sub>12</sub>ZnY phase) together with the Mg matrix. Fig. 1 is the XRD profile from the Mg<sub>97</sub>Zn<sub>1</sub>Y<sub>2</sub> alloy. The peaks of the Mg matrix phase acted as a calibration reference for other peaks. The intensity ratios deduced from the profile are 9.4, 7.1 and 9.4% for the dominant peaks of Mg<sub>24</sub>Y<sub>5</sub> (330), MgZn (701) and MgZn<sub>2</sub> (110) to Mg (100), respectively. This indicates that there is a large amount of Mg-Zn and Mg-Y precipitates in the studied alloys. It is well known that 2H-Mg has a hexagonal close-packed (*hcp*) crystal structure with the space group of P6<sub>3</sub>/mmc (194),  $a_{\text{Mg}} = 0.3209\ \text{nm}$  and  $c_g = 0.5211\ \text{nm}$ . The precipitate MgZn<sub>2</sub> has the same structure with 2H-Mg matrix,  $a_{\text{MgZn}_2} = 0.5253\ \text{nm}$  and  $c_{\text{MgZn}_2} = 0.8568\ \text{nm}$ . The precipitate Mg<sub>24</sub>Y<sub>5</sub> has a body-centered cubic (*bcc*) crystal structure with the space group of *I* $\bar{4}$ 3 *m* (217),  $a_{\text{Mg}_24\text{Y}_5} = 1.12\ \text{nm}$ . The JCPDS card numbers of them are 35-0821, 77-1177 and 31-0817, respectively. The MgZn phase is reported as a hexagonal structure with  $a_{\text{MgZn}} =$

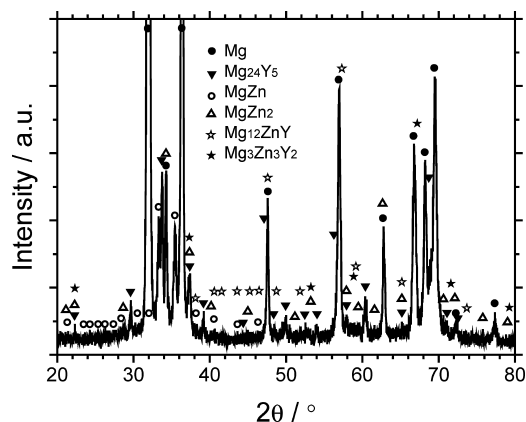


Figure 1 XRD profile from Mg<sub>97</sub>Zn<sub>1</sub>Y<sub>2</sub> as-cast ingots showing the Mg<sub>24</sub>Y<sub>5</sub> phase and two kinds of precipitates MgZn and MgZn<sub>2</sub> together with the LPS phase (18R-Mg<sub>12</sub>ZnY) and the Mg matrix. The intensity ratios deduced from the profile are 9.4, 7.1 and 9.4% of dominant peaks of Mg<sub>24</sub>Y<sub>5</sub> (330), MgZn (701) and MgZn<sub>2</sub> (110) to Mg (100), respectively.

2.557 nm and  $c_{\text{MgZn}} = 1.814\ \text{nm}$  from the No. 40-1334 JCPDS card.

The TEM observation shows that there are many dislocations and stacking faults in the grains of the matrix. The dislocations are always distributed along the grain boundaries, as shown in Fig. 2a. The dislocations can be identified by specimen tilting and a combination of two-beam bright-field and centered dark-field imaging techniques with several different operating diffraction vectors  $g$ . A method of dislocation identification and estimating dislocation density was established by Bailey and Hirsch [16]. It was reported that the grains with dislocations and stacking faults in Mg-Zn-Y alloys were actually a solid solution of *hcp*-Mg with Zn and Y [5–12]. A LPS phase, always with large-sized strip-like contrast, forms during

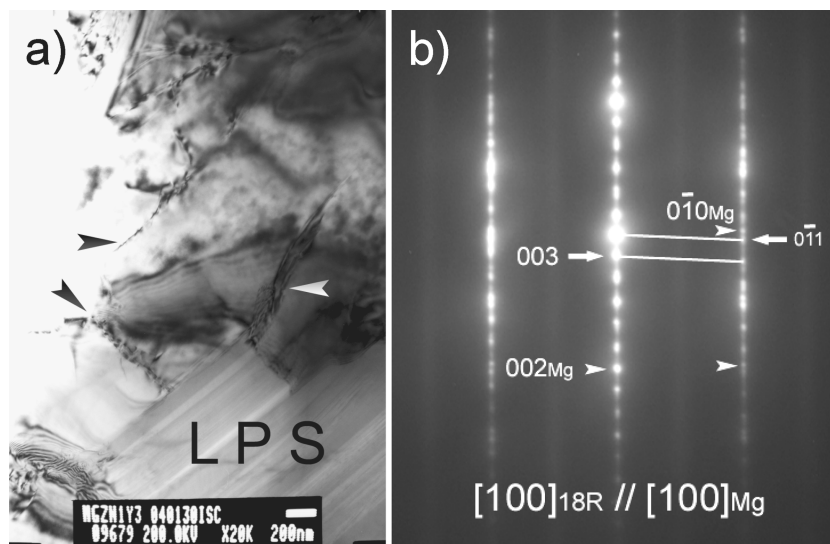


Figure 2 TEM bright-field morphology (a) in low magnification of a large-sized Mg grain in Mg<sub>96</sub>Zn<sub>1</sub>Y<sub>3</sub> as-cast ingots with dislocations distributing along the grain boundaries indicated by arrows, and the LPS phase on the bottom right corner with its EDP indexed as 18R-Mg<sub>12</sub>ZnY phase (b).

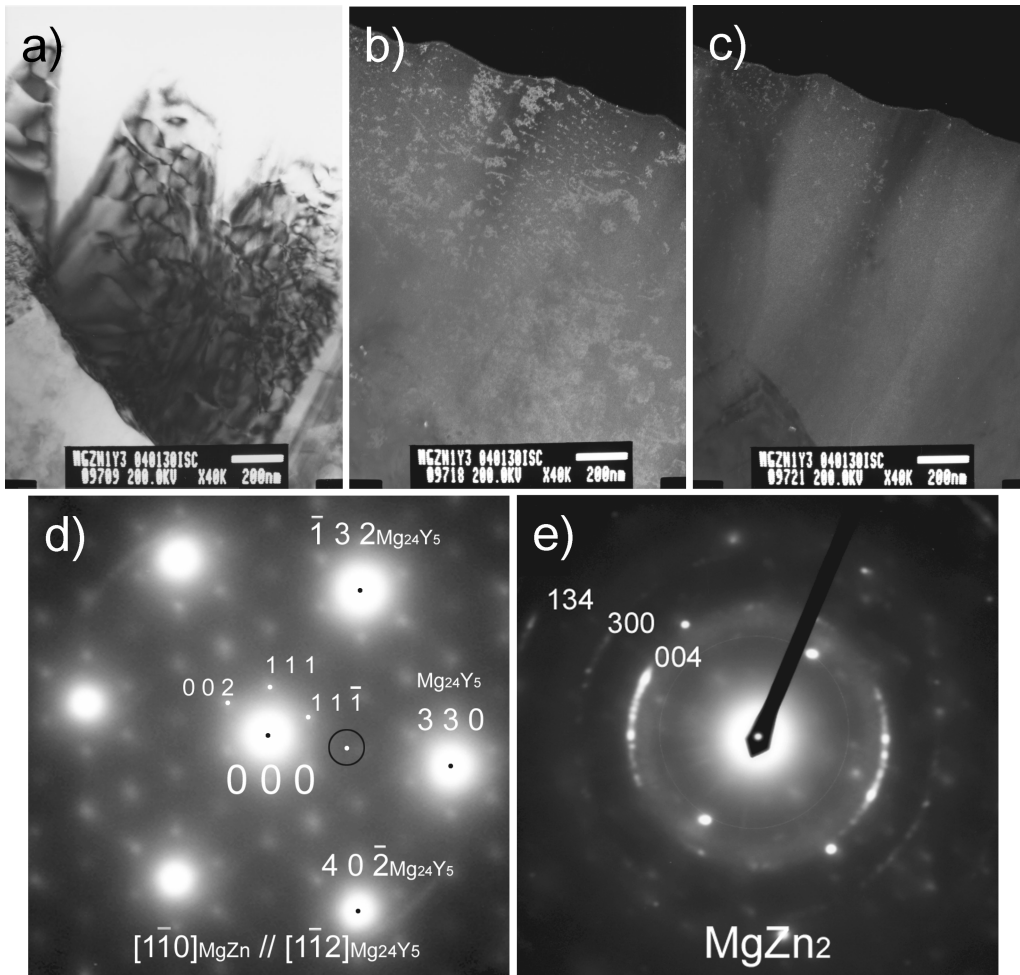


Figure 3 Bright-field image of  $\text{Mg}_{24}\text{Y}_5$  with dislocation network together with the Mg matrix shown as white triangles contrast in (a) in  $\text{Mg}_{96}\text{Zn}_1\text{Y}_3$  alloy. (b) is the DF image of MgZn precipitates from the  $(11\bar{3})$  spot in EDP shown in (d), where the big spots are indexed as  $\text{Mg}_{24}\text{Y}_5$  phase, and the small spots as MgZn phase. (c) is the DF image of  $\text{MgZn}_2$  nano-precipitates from the  $(004)$  ED ring in (e). The DF images show that the MgZn precipitates are distributed both in the  $\text{Mg}_{24}\text{Y}_5$  and the Mg grains while  $\text{MgZn}_2$  precipitates only in the  $\text{Mg}_{24}\text{Y}_5$  grains.

the cooling procedure of the solid solution [8–12]. The grain boundaries between the LPS phase and the Mg matrix are very clear. No amorphous phases are observed on the grain boundaries. Note that the LPS phase includes several phases. The LPS phase shown in Fig. 2a is actually the  $18R [(1, 1)(1, 3)]_3$  structure of  $\text{Mg}_{12}\text{ZnY}$  with the electron diffraction pattern (EDP) shown in Fig. 2b [17–22]. There is a small angle of about  $2^\circ$  between the planes of  $(0\bar{1}1)_{18R}$  and  $(0\bar{1}0)_{\text{Mg}}$ .

An  $\text{Mg}_{24}\text{Y}_5$  grain together with Mg matrix can be observed from the bright-field image shown in Fig. 3a. The dislocation network is distinguished clearly in the  $\text{Mg}_{24}\text{Y}_5$  grains. The two white triangular areas on the top are the Mg matrix. Fig. 3b is the two-beam centered dark-field (DF) image of MgZn precipitates from  $(11\bar{3})$  spot, marked by a black open circle, in the EDP shown in Fig. 3d. Fig. 3c is the DF image of  $\text{MgZn}_2$  nano-precipitates from the  $(004)$  electron diffraction ring shown in Fig. 3e. An inherent crystallographic relationship between the larger-

sized MgZn precipitate and the  $\text{Mg}_{24}\text{Y}_5$  phase,  $[1\bar{1}0]_{\text{MgZn}} [1\bar{1}2]_{\text{Mg}_{24}\text{Y}_5}, (11\bar{3})_{\text{MgZn}} (110)_{\text{Mg}_{24}\text{Y}_5}$  can be deduced from the combined EDP. The DF images show that the MgZn precipitates are distributed both in the  $\text{Mg}_{24}\text{Y}_5$ , and the Mg grains while  $\text{MgZn}_2$  precipitates only in the  $\text{Mg}_{24}\text{Y}_5$  grains. The size of the  $\text{MgZn}_2$  precipitates is much smaller than that of MgZn. It should be noticed that there is still some larger-sized  $\text{MgZn}_2$  in Fig. 3c due to the inclusion of some spots from  $\text{MgZn}_2$  precipitates in the objective aperture while obtaining the DF image of MgZn precipitates.

It is well known that precipitation strengthening is one of the main mechanisms for improving the mechanical properties of materials. In certain alloys, pre-existing dislocations provide preferred nucleation sites for metastable or equilibrium precipitates [23]. So it is suggested that the nano-sized precipitates, MgZn and  $\text{MgZn}_2$ , may improve the mechanical properties of the Mg-Zn-Y alloys investigated.

## 4. Conclusion

There is elemental segregation of Zn and/or Y in the  $Mg_{96}Zn_1Y_3$ ,  $Mg_{96}Zn_2Y_2$  and  $Mg_{97}Zn_1Y_2$  alloys studied in as-cast state. They form several precipitates of Mg-Zn, Mg-Y or Mg-Zn-Y phases. Nano-sized MgZn and MgZn<sub>2</sub> precipitates were found in the grains of solid solution of the alloys studied. The TEM observations show that MgZn precipitates are distributed in both the Mg matrix and Mg<sub>24</sub>Y<sub>5</sub> grains, which is another kind of typical precipitates in Mg-Zn-Y alloys. There is an inherent crystallographic relationship between the MgZn and Mg<sub>24</sub>Y<sub>5</sub> precipitates:  $[1\bar{1}0]_{MgZn} // [1\bar{1}2]_{Mg_{24}Y_5}$ ,  $(11\bar{3})_{MgZn} // (330)_{Mg_{24}Y_5}$ . The size of the MgZn<sub>2</sub> precipitates is much smaller than that of the MgZn precipitates. They are distributed only in the Mg<sub>24</sub>Y<sub>5</sub> grains, not in the Mg matrix. It is suggested that the nano-sized precipitates, MgZn and MgZn<sub>2</sub>, may improve the mechanical properties of the studied Mg-Zn-Y alloys.

## References

1. J. C. RAO, K. INOUE and Y. KAWAMURA, *Adv. Eng. Mater.* **7** (2005) 507.
2. R. F. DECKER, *Adv. Mater. Processes* **154** (1998) 31.
3. S. SCHUMANN and F. FRIEDRICH, in Proc. Int. 4th Int. Conf. on Magnesium Alloys and their Applications (Wolfsburg, Germany, 1998) p. 3.
4. Z. ZHANG, R. TREMBLAY, D. DUBÉ and A. COUTURE, *Canadian Metallurgical Quarterly* **39** (2000) 503.
5. J. B. CLARK and F. N. RHINES, *J. Met.* **209** (1957) 425.
6. K. NAIR, K. SUSEELAN and M. C. MITTAL, *Mater. Sci. Forum* **30** (1988) 89.
7. L. Y. WEI, G. L. DUNLOP and H. WESTENGEN, *Metall. Mater. Trans. A* **26** (1995) 1705.
8. Y. KAWAMURA, K. HAYASHI, A. INOUE and T. MASUMOTO, *Mater. Trans.* **42** (2001) 1172.
9. A. INOUE, Y. KAWAMURA, Y. MATSUSHITA, K. HAYASHI and J. KOIKE, *J. Mater. Res.* **16** (2001) 1894.
10. E. ABE, Y. KAWAMURA, K. HAYASHI and A. INOUE, *Acta Mater.* **50** (2002) 3845.
11. A. INOUE, M. MATSUSHITA, Y. KAWAMURA, K. AMIYA, K. HAYASHI and J. KOIKE, *Mater. Trans.* **43** (2002) 580.
12. D. H. PING, K. HONO, Y. KAWAMURA and A. INOUE, *Phil. Mag. Lett.* **82** (2002) 543.
13. C. H. CACERES and A. BLAKE, *Phys. Stat. Sol. (a)* **194** (2002) 147.
14. I. J. POLMEAR, "Light Alloys; Metallurgy of the Light Metals", 3rd Edn. (Arnold, London, 1995).
15. *Idem.*, *J. Metals* **20** (1968) 44.
16. J. E. BAILEY and P. B. HIRSCH, *Phil. Mag.* **5** (1960) 485.
17. Z. P. LUO, S. Q. ZHANG, Y. L. TANG and D. S. ZHAO, *Scripta Metall. Mater.* **28** (1993) 1513.
18. Z. P. LUO and S. Q. ZHANG, *J. Mater. Sci. Lett.* **12** (1993) 1490.
19. Z. P. LUO, S. Q. ZHANG, Y. L. TANG and D. S. ZHAO, *J. Alloys Compounds* **209** (1994) 275.
20. *Idem.*, *Scripta Metall. Mater.* **32** (1995) 1411.
21. Z. P. LUO and S. Q. ZHANG, *J. Mater. Sci. Lett.* **19** (2000) 813.
22. Z. P. LUO and H. HASHIMOTO, *Micron* **31** (2000) 487.
23. A. KELLY and R. B. NICHOLSON, *Prog. Mater. Sci.* **10** (1963) 149.